



# Use of aqueous polyvinyl alcohol in binder jetting of Inconel 718

Sourabh Paul<sup>1,2</sup> · Patrick J. Smith<sup>1</sup> · Kamran Mumtaz<sup>1</sup>

Received: 1 July 2024 / Accepted: 7 October 2024 / Published online: 17 October 2024  
© The Author(s) 2024

## Abstract

Binders used in binder jetting often pose health and environmental risks during processing and post processing operations. The print-heads which are used to deposit binder selectively on the feedstock are prone to clogging, despite the trend of print-heads being highly customised to suit different kinds of binders. These factors often hide the advantages of binder jetting as an additive manufacturing process, especially its scalability and its faster printing rates in comparison to powder bed fusion methods. The work presented here takes a step back and focuses on the development of an aqueous, polyvinyl alcohol (PVA)-based liquid binder that is easy to manufacture and store, safe to handle, and can be reliably jetted to print parts. The feedstock considered was Inconel 718, a nickel-based super alloy which can be effectively processed by binder jetting without niobium segregation. PVA was added to the Inconel 718 powder in dry, granular form to manufacture a modified feedstock. The study also investigated the role of molecular weight of the PVA used, sintering environments and post-processing methods like hot isostatic pressing (HIP) on process responses like part densification, tensile strength, and hardness. Three different types of PVA were chosen which had molecular weights 10,000 g/mol (low molecular weight or LMW), 26,000 g/mol (medium molecular weight or MMW), and 84,000 g/mol (high molecular weight or HMW). The compatibility of the liquid, aqueous PVA-based binders with virgin Inconel 718 was examined by measuring the contact angle. The liquid, aqueous binder having MMW PVA reported better wetting with the Inconel 718 powder with a wetting angle of 26.6 which was lower than the wetting angle of 42.4°, seen in case of a commercial resin-based binder. The green strength reported by the MMW PVA liquid binder was 220 kPa which was higher than the other two PVA-based liquid binders. Green parts, upon successful printing, were sintered at 1260 °C. It was observed that a part printed using MMW PVA had a densification of 96.16% when sintered in 99.98% by volume argon gas, which increased to 98.96% after undergoing HIP. The same part reported a densification of 88.69% when sintered in a 95% by volume N<sub>2</sub> and 5% by volume H<sub>2</sub> gaseous environment, which was later attributed to the uptake of nitrogen by the chromium present in Inconel 718, which prevented necking between particles. Tensile specimens printed using MMW PVA, sintered in a 99.98% argon environment, showed the highest ultimate tensile strength of 220 MPa, which increased to 1010 MPa after the HIP process, which can be compared to commercially available Inconel 718.

**Keywords** Binder jetting · Inconel 718 · Mechanical testing · Sintering

## 1 Introduction

### 1.1 Background and literature review

Additive manufacturing (AM), ubiquitously termed as 3D printing, is a group of manufacturing processes which are used to fabricate fully functional parts, often directly from a CAD model. These parts are built in an incremental layered manner. AM as a technology offers a host of advantages which include geometric flexibility, light weighting, efficient use of feedstock, lower tooling costs, and compressed design/development cycles [1–3]. Studies have also

✉ Sourabh Paul  
s.paul4@herts.ac.uk

<sup>1</sup> Department of Mechanical Engineering, University of Sheffield, Sheffield S1 3JD, UK

<sup>2</sup> School of Physics, Engineering & Computer Science, University of Hertfordshire, Hatfield AL10 9AB, UK

indicated that AM is a more sustainable and cost-effective manufacturing technique due to factors such as reduced material waste generation, localised material recycling, and improved product utilisation [4], which makes it a suitable process for materials which are expensive and are of strategic value.

Selective laser melting (SLM) is the most widely used AM process for the manufacture of parts having complex geometry, which are relevant to the aerospace and automotive sectors. Porosity, balling, shrinkage, and development of tensile residual stress are some of the challenges during processing of steel, titanium alloys, and nickel super alloys [5–7]. SLM of metals often uses structural supports to prevent distortion of parts and can require post-processing heat treatment to relieve thermally induced residual stresses [8, 9], which in turn increases the post processing time.

Binder jetting is an alternative AM technology where an adhesive binder fluid is selectively jetted on to a powder bed causing powder particles within the jetted region to loosely stick together forming a ‘green’ part. The printed ‘green’ part is then subjected to post-printing processing which may include stages like curing, debinding, and sintering. Binder jetting has demonstrated its capability of being a material agnostic processing technique, having the capability of printing metal alloys and ceramics with good resolution and without the problems encountered by SLM as discussed earlier [10]. Raza et al. processed Inconel 718 by SLM and obtained a coarser grain structure as compared to binder jetting, which was attributed to the formation of spherical MC type carbides and  $\gamma$ /Laves phases during SLM processing of Inconel 718 [11]. Niobium depletion and formation of brittle Laves phases were also observed during laser-based AM of Inconel 718, which changes the alloy composition and is detrimental to the mechanical properties of the fabricated parts [12–14]. The segregation of niobium can be avoided during the post processing of the green parts fabricated by binder jetting by sintering them at 1260 °C in an argon environment with a ramping rate greater than 10 °C/min [15].

Currently, commercial binder jetting systems depend on using liquid binders which use solvents like phenolic resins and diethylene glycol. Different solvents require print heads to be customised to suit their rheological properties. The customisation approach increases production costs and resistance to standardisation of BJT in industry. The use of phenolic resins also causes clogging of nozzles during periods of downtime [16]. Commercial binders composed of furan or alkyl-based phenolic resins [17] are expensive, require substantial investment in health and safety, pose disposal problems, and require specialised ventilation units. The problems highlighted justify efforts to investigate new materials as potential alternative binders which would be easier to handle in any state, readily available, and low environmental impact upon disposal. A feasible way this can

be achieved is by customising the feedstock powder with a generic dry binder and additives. The homogeneously mixed binder would then be converted into a green part by the deposition of a generic solvent like diethylene glycol, alcohol, or water. This strategy would allow customised feedstock powder to be produced that can then be processed using low cost off the shelf print heads. These would not require any form of customisation and can be easily replaced upon damage, without contributing significantly to the cost of technology.

Polyvinyl alcohol (PVA) can be potentially, a suitable alternative to existing commercial resin-based binders in binder jetting of metals. It is a water-soluble synthetic polymer which is chemically stable, has good adhesive properties and is known to be safe for use, and does not require any special training or equipment for handling. The work of Hallensleben et al. suggested that aqueous solutions containing up to 5% of PVA by weight is non-toxic to aquatic life [18]. This indicates that PVA as a chemical compound has a lower environmental impact. The toxicological information of PVA and furan, a common component used in commercial resin-based binders, indicates that PVA is a safer compound to handle [19, 20]. This justifies investigation of the suitability of PVA as a binder. The compatibility of water with PVA, its abundant availability, and ability to wet surfaces vindicates its suitability as a solvent.

Miyanaji et al. have investigated the wettability of commercial binder on a powder bed of stainless steel (SS 420) as the contact mechanics and infiltration of binder within the powder bed affect the bonding between the powder particles and the inter-layer bonding, indicating the importance of wettability in binder jetting [21].

PVAs are usually chemically consistent in their properties; however, different molecular weights of the same polymer reflect on the physical properties like solubility in water [22]. It was prudent to investigate the role of molecular weight of PVA on its suitability as a binder in the form of analysis of process responses like wettability with the metal substrate and porosity.

## 1.2 Gaps in research literature and summary

The study explores the use of binder jetting as an alternative AM method to process Inconel 718 to circumvent problems like tensile residual stress and niobium segregation at the grain boundaries, which are the characteristic challenges faced during SLM-based processing of Inconel 718. There is insufficient literature which has reported the processing of Inconel 718 using binder jetting. Preliminary work on processing of Inconel 718 using binder jetting has suggested better control of microstructure of sintered parts in comparison to SLM. The work also looks at developing a generic, liquid binder composed of PVA and water and evaluating its suitability in printing green parts of Inconel 718. While

PVA and long-chain molecule-based compounds have been explored as liquid binders for ceramics and some grades of steel [23, 24], they remain unexplored as a suitable binder candidate for processing Inconel 718. A modified feedstock has been used, composed of Inconel 718 powder and dry, powdered PVA to maintain the non-toxicity of the liquid binders, increasing its ease of handling, storage, and disposal. The quality of printed ‘green’ parts has been interconnected to wettability and stability of the liquid binder with the metal powder, hence the choice of de-ionised water as a solvent throughout the study.

## 2 Materials and methods

### 2.1 Preparation of modified feedstock

PVA beads (Alfa Aesar, Heysham, UK) of 10,000, 26,000, and 84,000 g/mol of 99% purity were converted into fine powder by ball milling them in a cryogenic micro mill (CryoMill, Retsch, Haan, Germany) for 12 h. The PVA powders having molecular weights of 10,000, 26,000, and 84,000 g/mol would be referred to a low molecular weight (LMW), medium molecular weight (MMW), and high molecular weight (HMW) samples respectively throughout the rest of

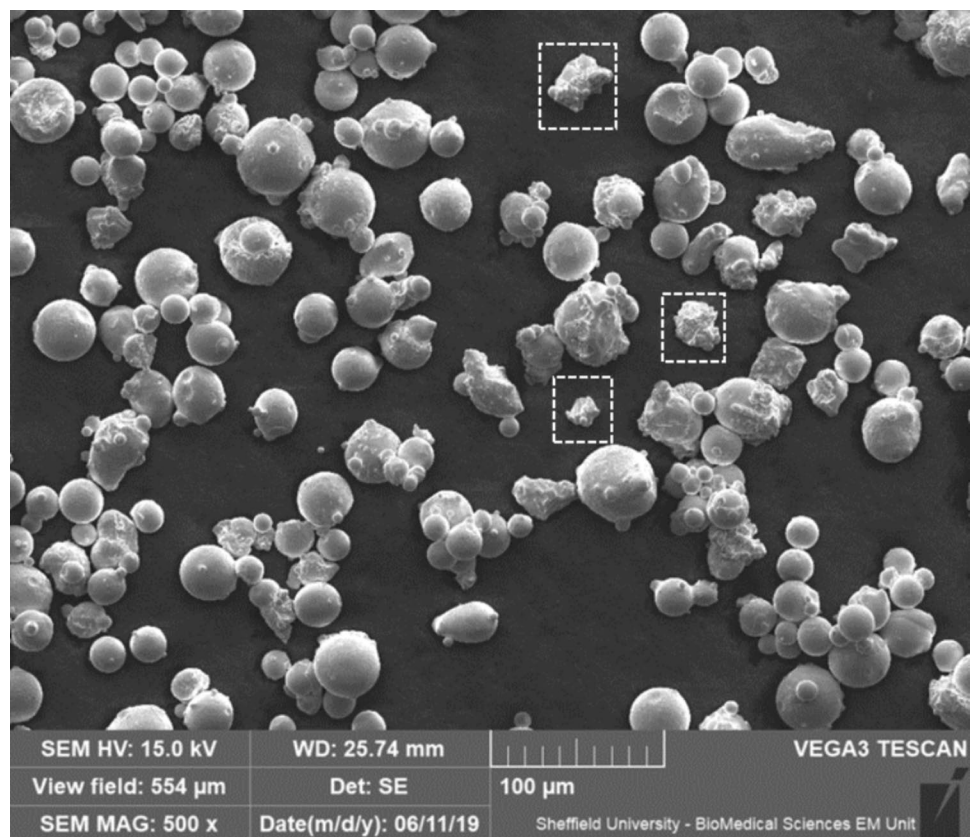
this study. The powders were then used as a raw material to prepare the modified feedstock and the liquid binder.

The modified feedstock was prepared by mixing Inconel 718 powder (particle diameter 15–45  $\mu\text{m}$ , LPW Technology, Widnes, UK) with each of the LMW, MMW, and HMW PVA powders in a high-speed mixer (DAC800FVZ, Synergy Devices, High Wycombe, UK) at 600 RPM for 60 min. For each type of PVA based on molecular weight, two different compositions of feedstock were prepared, namely, 5% and 10% by weight, respectively. Figure 1 shows a micrograph taken using a scanning electron microscope (SEM), which highlights the modified feedstock containing 5% wt. MMW PVA which is homogeneously dispersed in Inconel 718 powder.

### 2.2 Powder rheology of the prepared feedstock

The permeability and the variable flow rate (VFR) of the different feedstock were measured using an FT4 powder rheometer (Freemantech, Tewkesbury, UK). The parameters were measured in accordance with ASTM D7981-20 standard on compaction of powders [25]. This standard was adopted in favour of more widely accepted standards like ASTM B964-23 (using a Carney funnel) and ASTM B213 (using a Hall funnel) due to the compaction which powders undergo during the powder spreading process in binder

**Fig. 1** SEM micrograph of modified feedstock. Particles demarcated by dashed squares indicate PVA particles mixed in an Inconel 718 feedstock



jetting. Virgin Inconel 718 was initially characterised as a benchmark to understand the effect of the addition of different PVA powders on the spreadability of the modified feedstock. The rheological studies were based on the rotation of a stainless-steel blade which would be inserted into a cylindrical glass vessel of 25 mL containing a sample of the feedstock. The resistance to dynamic flow experienced by the rotating blade due to the powder present in the vessel would be directly proportional to the VFR. The methodology was best described by the work of S ogaard et al. [26], whose work evaluated the feasibility of using the FT4 rheometer as a reproducible characterisation method.

### 2.3 Preparation and characterisation of liquid binder—aqueous solution of PVA

The liquid binder was made by dissolving the powdered PVA in deionised water slowly using an overhead stirrer (T25 Ultra Turrax, Oxford, UK) while maintaining the solution at 80  C. Three different concentrations of liquid binder were prepared for LMW, MMW, and HMW PVA, namely, 0%, 5%, and 10% by weight. The concentration values in either the liquid binder or modified feedstock were taken effectively as 5% and 10% to ensure that the total PVA content was within the toxicity levels as discussed in Sect. 1.1.

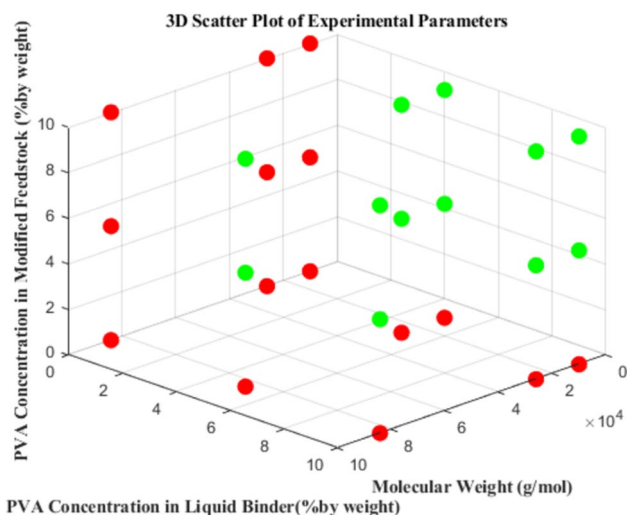


Fig. 2 3D scatter plot of experimental parameters

**Table 1** Summary of attempts to print green parts with variation in composition of PVA in the liquid binder and modified feedstock

Liquid binder Conc. (→)	0% wt. PVA	5% wt. PVA	10% wt. PVA
Feedstock Comp. (↓)			
0% wt. PVA	Green part disintegrated	Green part disintegrated	Liquid binder did not jet
5% wt. PVA	Green part disintegrated	<b>Part printed, cured</b>	Liquid binder did not jet
10% wt. PVA	Cured part disintegrated	Cured part disintegrated	Liquid binder did not jet

Figure 2 is a scatter plot where each dot represents the coordinates  $(x,y,z) \sim (\text{molecular weight, PVA concentration in liquid binder, PVA concentration in modified feedstock})$ . The dots are coloured red whenever the amount of PVA is 0%, either in the liquid binder or the modified feedstock, as these sets of experimental parameters produced fragile parts which collapsed, often under their own weight. This was experimentally observed as has been discussed at length in Table 1.

Rheological characterisation of the liquid binders included measurement of their surface tension and dynamic viscosity. The surface tension of the liquid binders was measured using a tensiometer with a Wilhelmy plate attachment (K20, Kr uss GmbH, Germany), and the dynamic viscosity was measured using a DV2T Brookfield viscometer.

### 2.4 Sessile drop test of liquid binders

The compatibility of the different binders with the modified feedstock was initially assessed by performing sessile drop tests in accordance with ASTM D7334 – 08 (2022) [27], where the contact angle  $\theta$ , made between the droplet and the feedstock spread on a powder bed, was measured after 30 s of droplet deposition. A major deviation from the ASTM standard was the use of a powder substrate instead of a solid surface. This was done to simulate conditions of the adhesive wetting the powder during binder jetting and has been done in multiple studies [28]. The wettability of the different PVA-based binders was compared with a binder which is used in commercial binder jetting systems. The wettability test consisted of depositing a droplet of 1  $\mu\text{L}$  using a variable adjustable volume pipette (Eppendorf, Germany) on a pocket of depth 200  $\mu\text{m}$ . The droplets were generated at a height of 2 mm from the surface of the powder bed. A Levenhuk DTX 50 digital microscope was used to capture the droplet deposition phenomenon at a rate of 200 frames per second. The contact angle was calculated by drawing a tangent to the drop profile at the common point of contact of the three phases which was done using an open-source image analysis software, ImageJ as used in previous work of Zavala-Arredondo et al. [29].

## 2.5 Processing, post-processing, and testing of parts

Dog bone tensile samples were printed using a commercial inkjet system (Jetlab 4xl, Microfab Technologies, Texas, US) where the binder was deposited on the modified feedstock with a layer thickness of 200  $\mu\text{m}$ . The dog bones were printed following the guidelines of ASTM F3055-14a with the dimensions being reduced by a factor of two to fit the sample in the powder bed of the Jetlab 4xl system. Printing capacity was gradually built up as shown in Fig. 3. Green parts were printed in line with ASTM B312 for the green strength trials. A single printhead (MJ-AT-01, Microfab Technologies, Texas, US) having an orifice diameter of 60  $\mu\text{m}$  was used to deposit droplets onto the feedstock in a ‘drop on demand’ manner. The binder was dispensed at a voltage of 27 V, pulse width of 21  $\mu\text{s}$ , and an operating frequency of 250 Hz. The traverse speed of the printhead during printing was maintained at 10 mm/s. This process was repeated across multiple layers to create a ‘green’ part which was then cured in an oven at 60  $^{\circ}\text{C}$  for 12 h in a low-temperature oven (3608-6CE, Thermo Scientific, Waltham, US) and then sintered in a tube furnace (LTF 14/25/180, Lenton Furnaces, Hope, UK). The temperature profile is specified in Fig. 4. Two different purging environments were used: (a) pure argon from start

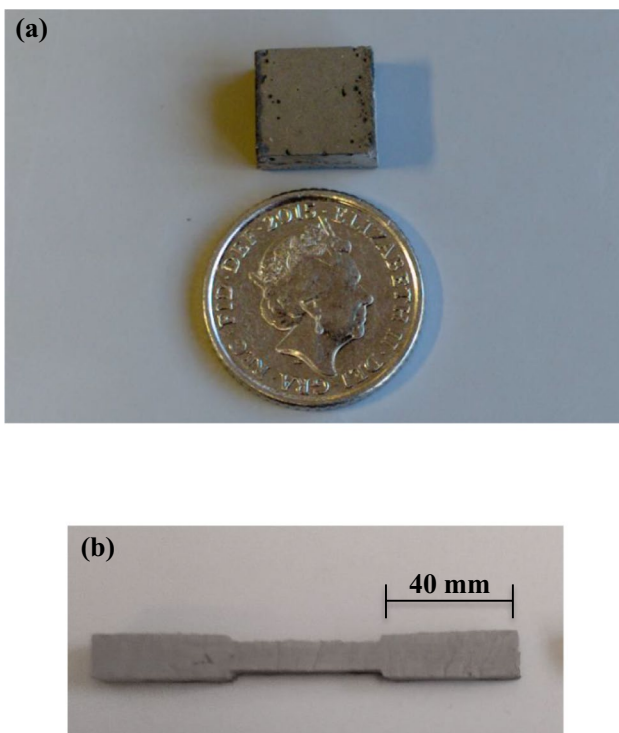


**Fig. 3** Sintered specimens; **a** cubical; **b** tensile dog bone

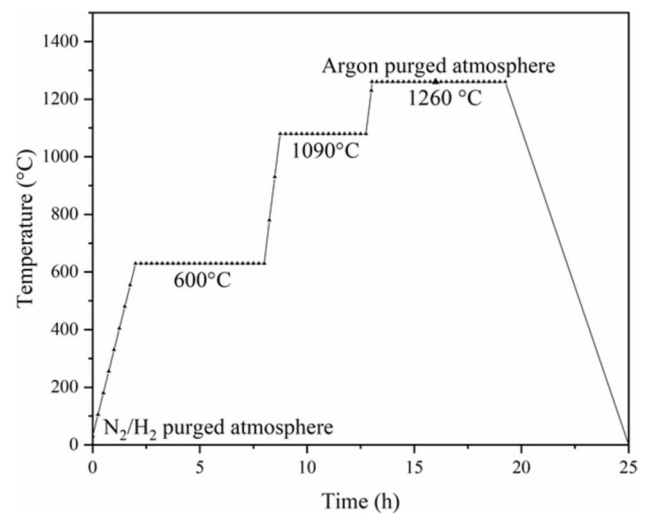


**Fig. 4** Thermal profile of the sintering process of the green parts [30]

to finish; (b) 95%  $\text{N}_2$  + 5%  $\text{H}_2$  till 1260  $^{\circ}\text{C}$  and then argon for the final sintering at that temperature [30].

The binder present in the green part was removed mostly at 600  $^{\circ}\text{C}$ , following the ASTM E1131-20 standard for thermoplastics before the part was pre-sintered and sintered at 1090  $^{\circ}\text{C}$  and 1260  $^{\circ}\text{C}$ , respectively. Thermogravimetric analyses of the different binders in their solid, granular state at 600  $^{\circ}\text{C}$  and 1260  $^{\circ}\text{C}$  were conducted respectively in an argon environment.

A hot isostatic press (AIP 10-30H, AIP Inc., Ohio, US) was used to compress the sintered parts in a bid to see its effect on process responses including porosity, tensile strength, and hardness. The samples were heat treated at 1200  $^{\circ}\text{C}$  and 120 MPa for 3 h and was allowed to cool to room temperature within the press. Tensile specimens of samples sintered solely in argon were processed in hot isostatic conditions for reasons explained in Sect. 3.8.1. Cubical samples of dimensions  $10 \times 10 \times 10 \text{ mm}^3$  were HIPed for the other combinations for hardness testing so that all the samples could be processed in a single HIP cycle.

Tensile testing of the printed dog bones was conducted using a Universal Testing Machine (50 ST, Tinius Olsen, Red Hill, UK) with a 50 kN load cell and a clip-on axial extensometer (Model 3542, Epsilon Technology Corporation, Jackson, US) which measured the strain until the point of fracture. The strain rate was maintained within the range of 0.003–0.007 mm/mm/min as per the specifications of ASTM F3055-14a ensuring that the sample failed within 1 min. Green strength of the printed samples was conducted by measuring the deflection of the green parts using a standard flexural strength measurement setup fitted onto the same Universal Testing Machine with a rate of displacement of 1 mm/min.

The hardness of the samples was measured using a HM-210 testing machine manufactured by Mitutoyo with an incident load of 10 kgf. The hardness was measured in SI units.

The phase analysis of the samples was completed using an X-ray diffractometer (Empyrean system, Panalytical BV, Almelo, Netherlands). Cu-K $\alpha$  radiation was used with the Cu tube set at 40 kV and 45 mA. An X ray mask of 1 mm width was used to filter the incoming X rays which were then sent outwards via a divergent slit having a width of 2 mm. The scanning was performed between 30 and 100° with an incremental step of 0.1°. The X ray beam was passed through a parallel plate collimator after diffraction, and its intensity was monitored by a PIXcel detector which was set at 0D mode.

### 3 Results and discussion

#### 3.1 Thermal behaviour of binder

One of the parameters which would determine the suitability of a binder is the ease with which it is debound or removed from the green part. This step can be achieved by either solvent based or thermal debinding. The specimens in this study were thermally debound at 600 °C according to the ASTM E1131-20 standard [31]. PVA is an organic material and improper debinding may result in presence of carbon residue within the part which would compromise the composition of the alloy. Thermogravimetric analysis of the binder was performed at both 600 °C and 1260 °C to quantify the residue left behind due to thermal degradation of PVA, as seen in Figs. 5 and 6. The final plot at 600 °C

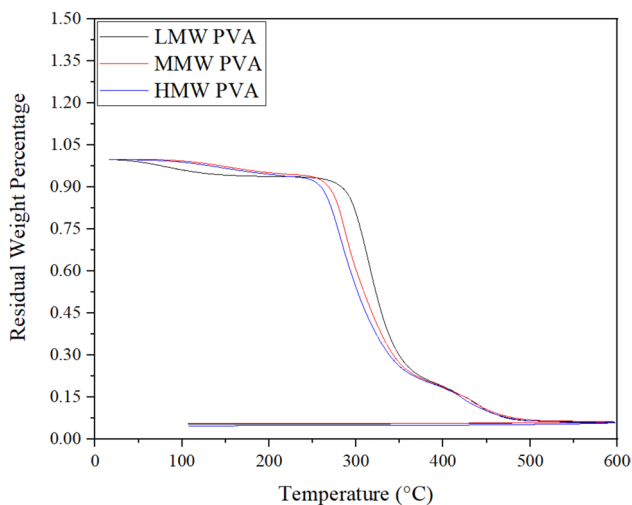


**Fig. 5** Thermogravimetric analysis of different binders in their granular form till 600 °C

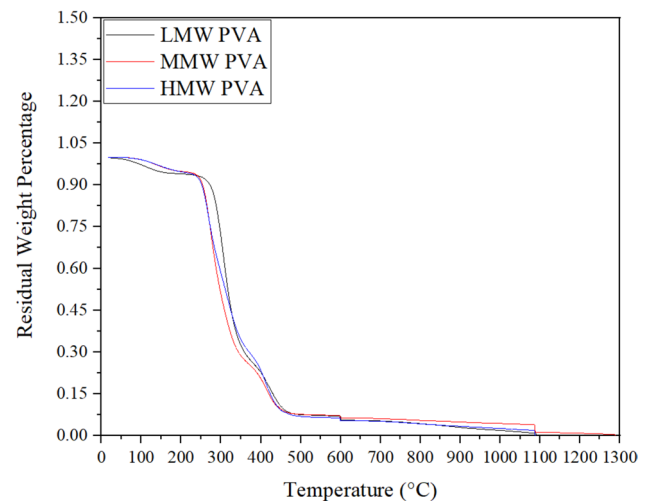


**Fig. 6** Thermogravimetric analysis of different dry binders till 1260 °C

is suggested that the residue present was 7.5% by weight which reduced to 0.03–0.04% by weight during the final sintering step which happened at 1260 °C. While there is no literature available for Inconel 718, Cai et al. reported presence of 0.05–0.06% by weight of carbon at 1380 °C while processing SS316L using PVA based binders [24].

#### 3.2 3.2. Printability trials

The effect of the composition of the modified feedstock and the concentration of PVA in the liquid binder on build quality and structural integrity of the parts was investigated by trial and error. The addition of excessive or a minimal amount of PVA in liquid binder during the printing process could lead to problems such as poor surface quality and lack of inter particle bonding respectively as discussed extensively by Lores et al. in their review [32]. Table 1 describes the trials which were performed to obtain an optimum amount of PVA within the liquid binder as well as in the modified feedstock. It was observed that the green part usually disintegrated when the combined PVA content in liquid binder and modified feedstock was low, indicating poor inter particle bonding. A higher presence of PVA in the modified feedstock resulted in the crumbling of the part after the curing process. This could be attributed to the lower water content in the binder, which led to drying out of the part in the curing oven. The trend exhibited in Table 1 was similar across PVAs of all three different molecular weights used. It was understood that the PVA content in the liquid binder and the modified feedstock would have to be 10% and 5% by weight, respectively, independent of molecular weight.

### 3.3 Rheological characterisation of modified feedstock

The ability of the feedstock to spread easily is important in AM processes like binder jetting. Any undue resistance in the flow of the feedstock would be detrimental to the entire printing process and would compromise with the tight dimensional and geometric tolerances which are expected from most AM methods. The studies of Clayton et al. suggested that the suitability of a feedstock for any AM process required the measurement of different parameters like permeability and specific energy [33]. Studies have also indicated that the FT4 powder rheometer measured properties like VFR and permeability in a consistent manner [34].

Figure 7a, b depicts the variation of permeability and VFR respectively of different feedstock, including pure Inconel 718. All the modified feedstock containing PVA of

different molecular weights had increased permeability in comparison to pure Inconel 718. The total energy of pure Inconel 718 increased with every iteration of the stainless-steel blade as it interacted with the sample present within the cylindrical chamber. The feedstock composed of Inconel 718 and HMW offered the least resistance to the moving blade over twelve iterations but offered limited improvement in permeability. The combination of Inconel 718 and MMW PVA had the highest permeability but displayed an inconsistent trend during the VFR experiments. The conflicting values led to a measurement the shear stress of the different feedstock to understand the behaviour of the entire consolidated powder bed, when a fresh layer of powder is being spread. Figure 7c depicts the variation of shear stress over a range of standardised normal stresses, and it was interesting to note that the variation between the HMW and MMW feedstock was minimal, and

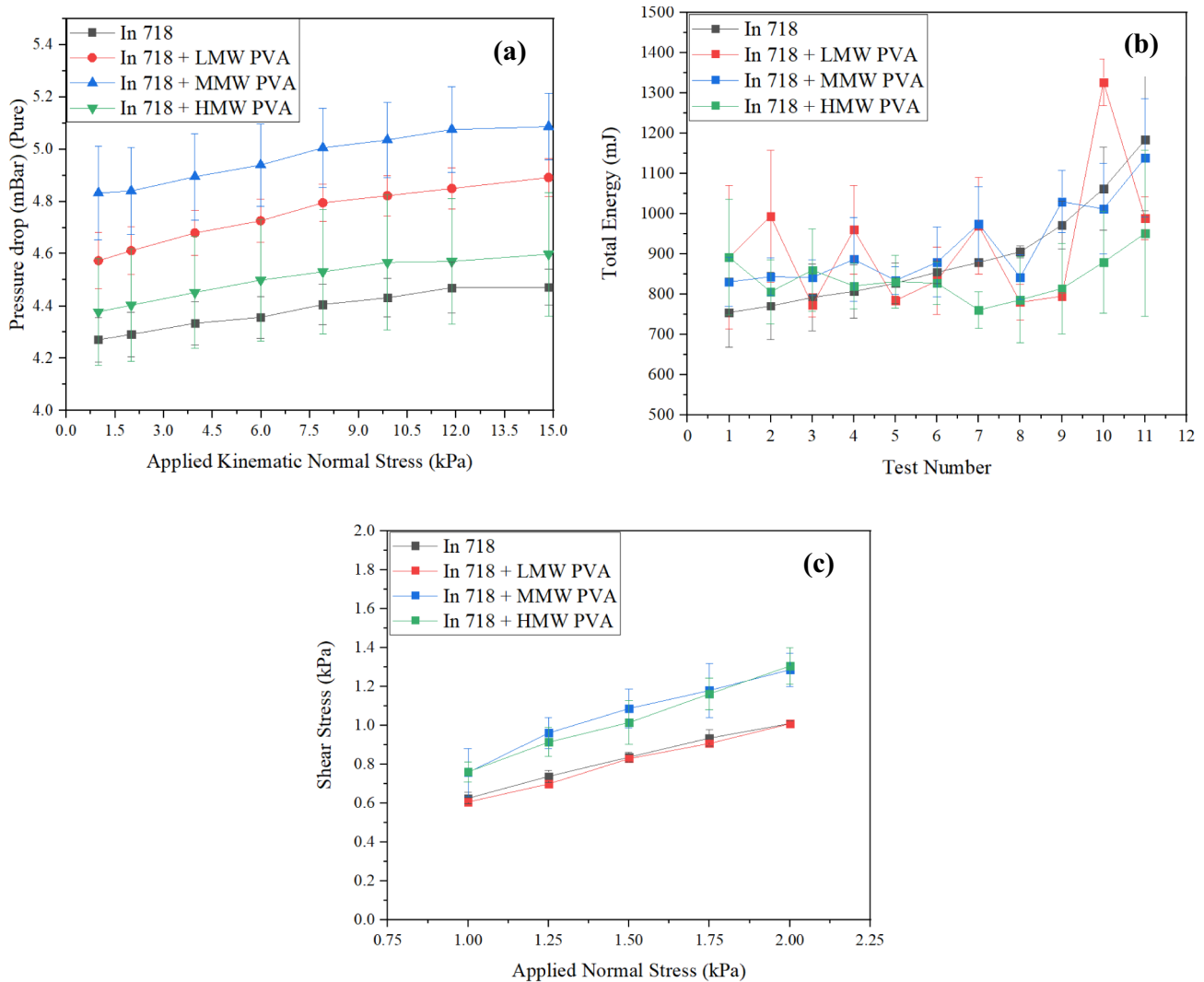


Fig. 7 Rheological evaluation of different feedstock: **a** permeability; **b** variable flow rate (VFR); **c** shear stress

both behaved similarly throughout the range of different applied normal stresses. Pure Inconel and the combination of Inconel 718 and LMW yielded high shear stress, which would indicate poor powder spreadability and inconsistent layer thickness.

### 3.4 Rheological characterisation of liquid binder

It was observed that a liquid binder containing 5% PVA by weight and a feedstock containing 5% of powdered PVA by weight was a suitable combination. However, the effect of molecular weight of PVA was unknown. The studies of Mohsen-Nia et al. indicated that the rheological properties of PVA were dependant on its molecular weight and degree of polymerisation [35]. Figure 8a, b depicts the dynamic viscosity and surface tension of the liquid binders containing LMW, MMW, and HMW, respectively.

The liquid binders have a higher starting value of dynamic viscosity compared to deionised water as seen in Fig. 8. The values of dynamic viscosity of the LMW, represented by the red lines, are the lowest of all the liquid binders, which would suggest a better ability to penetrate the powder bed and wet the Inconel 718 powder. However, it was important to ensure consistent jetting of the binder to understand the role of molecular weight in the wetting of the powder particles evenly to ensure a strong green part. The Ohnesorge number is a dimensionless number which has traditionally been used to understand if a liquid is jettable from a printhead of fixed diameter [36]. The Ohnesorge number ( $Oh$ ) can be calculated as given in Eq. (1).

$$Oh = \frac{\mu}{\sqrt{\sigma \rho L}} \quad (1)$$

where  $\mu$  is the dynamic viscosity,  $\sigma$  is the surface tension,  $\rho$  is the density of the liquid being jetted by the printhead, and  $L$  is the diameter of the printhead. The  $Oh$  was calculated for the liquid binders made of 5% concentration of LMW, MMW, and HMW, respectively. However, it is usually represented in the form of its reciprocal, which is termed as the  $Z$  number, as provided in Eq. (2).

$$Z = \frac{1}{Oh} \quad (2)$$

The studies of Derby et al. suggested that the range of the  $Z$  number for stable jettability should be such that  $Z \in [1, 10]$ . The range of the  $Z$  for the three liquid binders was calculated to be in the range of 74 to 78, but consistent jetting of the liquid binders was observed as has been also reported by Tekin et al. and Vadillo et al. [37, 38].

### 3.5 Wettability analysis

The selective addition of binder across the powder bed is required to essentially ‘glue’ together powder particles near each other and create near net shape components with sufficient temporary structural integrity (allowing it to be gently handled as a ‘green’ part) before undergoing further post-process furnace cycles (binder burnout and component densification through sintering). The structural integrity of this ‘green’ component and geometric accuracy/resolution is directly dependent on the wettability of the liquid binder jetted onto the binder [39, 40].

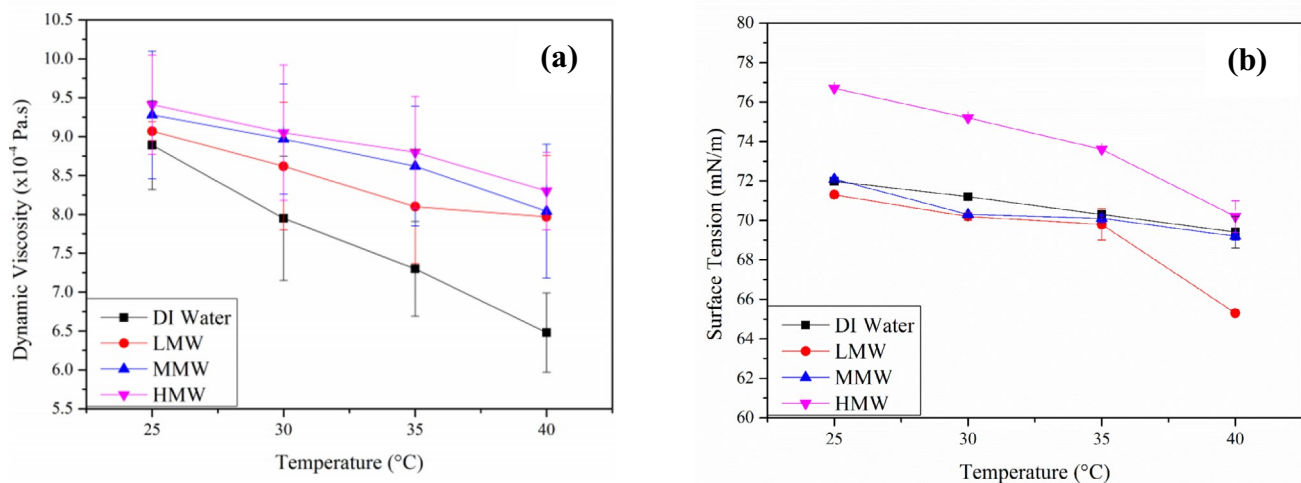


**Fig. 8** Temperature based variation of **a** dynamic viscosity and **b** surface tension of different liquid binders, bench marked against deionised water

Measurement of the contact angle formed by de-ionised water when dropped on a powder bed of modified feedstock with PVA of variable molecular weights was undertaken. It was observed that the water completely percolated into the porous powder bed instantaneously and well before 30 s had elapsed. This was a common observation made when the experiment was repeated with the different types of feedstock consisting of PVA granules of different molecular weights.

Figure 9a through d depicts the interaction between virgin Inconel 718 feedstock and a droplet of aqueous binders with LMW, MMW, and HMW grades of PVA along with a commercial resin-based binder. It was observed that the binders with dissolved MMW and HMW PVA had better wettability than the commercial binder. An interesting observation was that the LMW binder had the highest wetting contact angle. The interaction between the different PVAs and the powder substrate can be explained based on their molecular weight and length of the polymeric chain. The molecular weight of the monomeric unit of PVA,  $[\text{CH}_2 - \text{CH}(\text{OH})]$  is 44 g/mol. It can be calculated that the low, medium, and higher molecular weight samples of PVA had 227, 590, and 1909 units of this basic PVA structure. There are usually a few distinct types of interactions in an aqueous solution of conventional, atactic PVA: (a) hydrogen bonding between two adjacent  $-(\text{OH})$  groups in the same chain, (b) hydrogen bonding of the  $-(\text{OH})$  group with the surrounding water molecules, and (c) Van der Waals interaction between the basic  $[\text{CH}_2 - \text{CH}(\text{OH})]$ , where the H atoms donate its sole

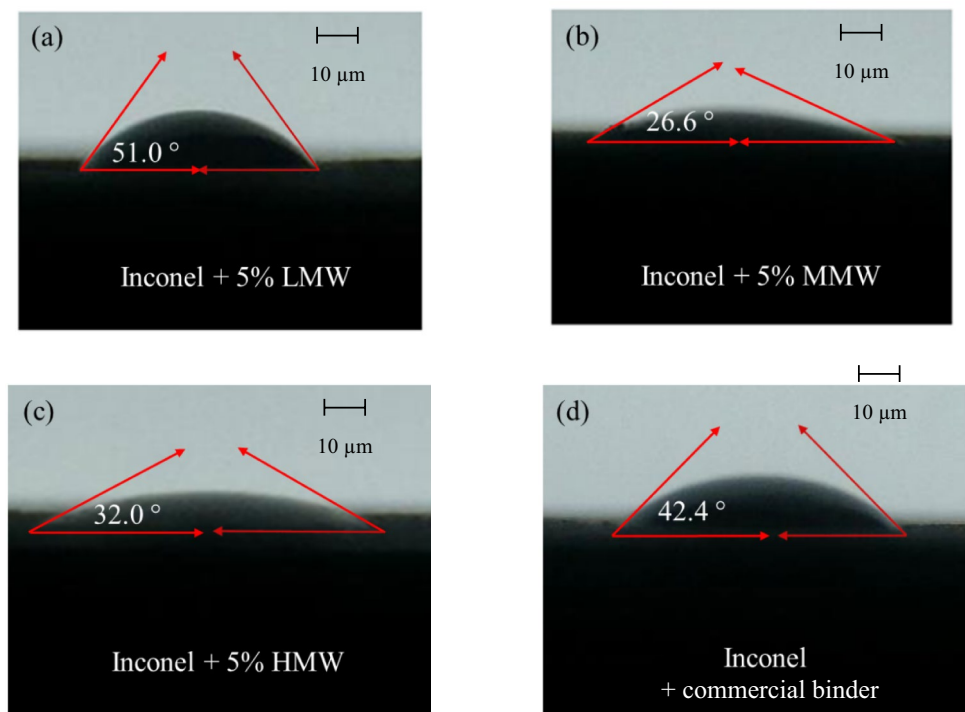
electron to the C atom [41]. Gravity can also be a physical factor which could affect the outcome of the sessile droplet test. The kinetic energy possessed by the droplet while hitting the surface of the powder bed would result in substantial deformation of the powder bed which would be detrimental to the printing process. It would also lead to loss of control on droplet deposition process due to its rebound or disintegration. The volume of the droplet and the height at which the droplet was released were kept minimal to prevent any distortion of the powder bed or the droplet.

The intramolecular hydrogen bonding tends to slightly dominate the other forms of interaction in dilute solutions of long chained PVA at low temperature and encourages intramolecular cross linking [41, 42], which decreases the interaction between the PVA chain and surrounding molecules which allows the solvent (in this case, distilled water) to spread more on a surface. When the drop of binder impinges on the modified feedstock, the water can potentially start interacting with the PVA granules present within the modified feedstock. No immediate dissolution of the PVA would occur with the aqueous component of the droplet at room temperature. Their interaction could be captured by the Flory–Huggins equation [43, 44], which is:

$$\Delta G_m = RT [n_1 \ln \phi_2 + n_2 \ln \phi_1 + n_1 \phi_2 \chi_{12}]$$

The right-hand side is dependent on the number of moles  $n_1$  and volume fraction,  $\phi_1$  of the solvent (which is water in this case), the number of moles  $n_2$  and volume fraction  $\phi_2$ ,

**Fig. 9** Wetting angle produced by a droplet of liquid binder (composed of different molecular weights of PVA) on a substrate of virgin Inconel 718 feedstock at the instance of 30 s from initial contact: **a** water + 5% LMW, **b** water + 5% MMW, **c** water + 5% HMW, and **d** commercial binder



of the solute (PVA).  $\chi_{12}$  is termed as the mixing parameter.  $R$  is the gas constant, and  $T$  is the temperature in Kelvin. The calculations suggested negative values of  $\Delta G_m$  for PVA which became less negative in value with the increase in the molecular weight of the PVA. The values, which are provided in the Appendix, indicate that the immediate interaction between the aqueous component of the binder droplet and the granular PVA in the modified feedstock is negligible due to the low values of  $\Delta G_m$ . When the temperature is raised above room temperature, the value of  $\Delta G_m$  implies increased spontaneity of the dissolution of dry PVA into water. The dry PVA dissolves slowly into the moisture present in the green part during the curing process in the oven at 60 °C, thus increasing the robustness of the green part over the curing process.

Figure 10 summarises Fig. 9 in a quantitative manner, where it is observed that the medium and high molecular weight PVAs have lower contact angle as compared to the resin-based binder used by commercial binder jetting systems.

### 3.6 Green strength of printed parts

Miyanaji et al., in their review, mentioned the importance of printing robust green parts to achieve good mechanical properties once the parts are sintered [45]. Zhou et al. performed compression tests on green parts made of hydroxyapatite, using maltodextrin and commercial thickening agents based on PVA as candidate binders [46]. Figure 11 depicts the deflection of the samples printed using the various feedstock. The green part printed using MMW PVA showed the highest flexural strength, withstanding a maximum load of 140 N for a deflection 0.4 mm. The parts

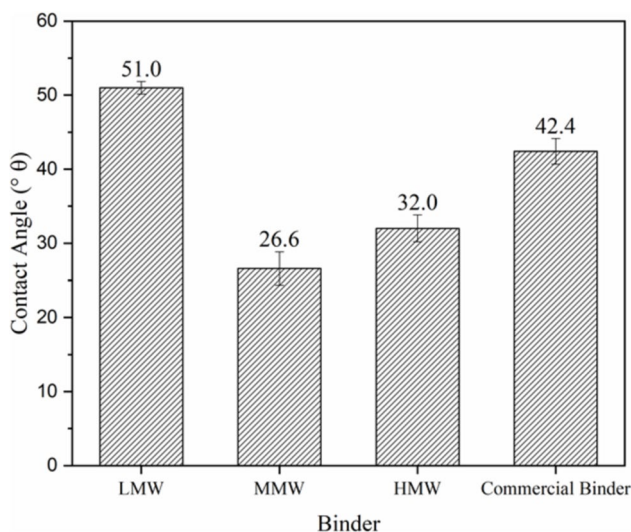


Fig. 10 Summary of wetting angle measurement experiments

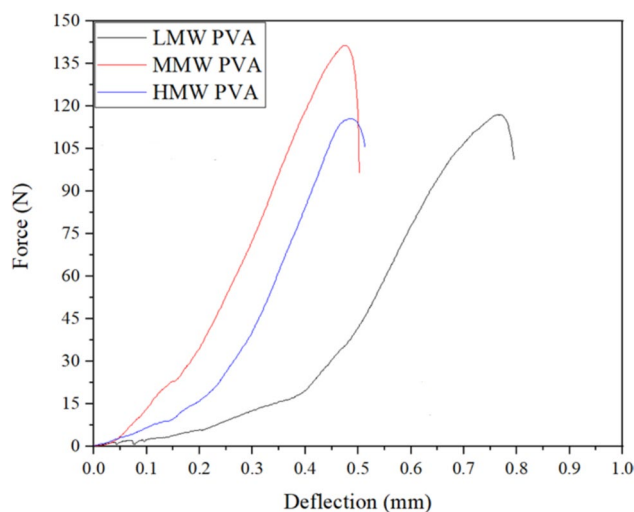


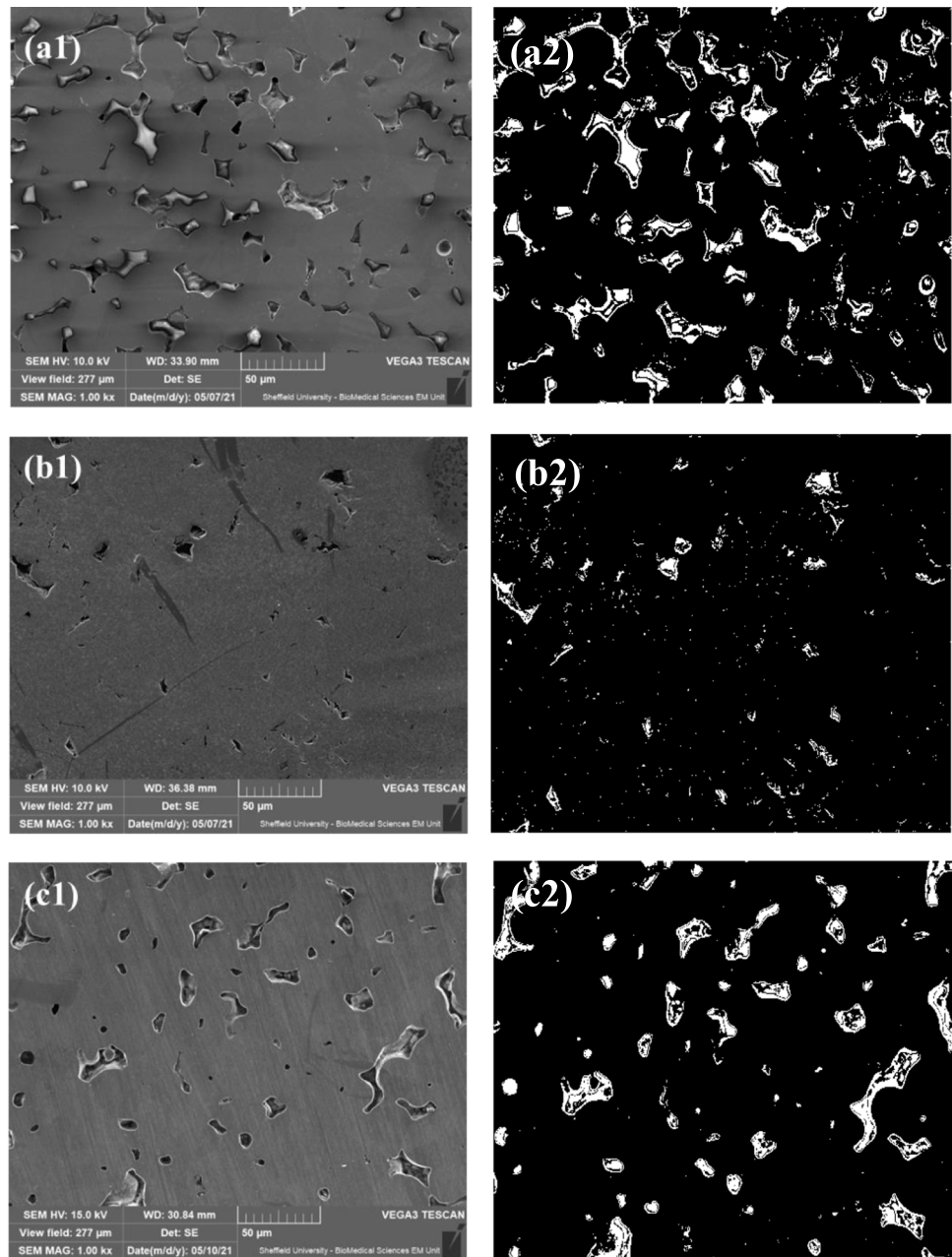
Fig. 11 Force vs. deflection of green parts prepared with different feedstock and binders

printed using HMW PVA also shows similar behaviour but underperforms only marginally compared to MMW. This is because of the better wetting exhibited by the MMW and HMW PVAs on their corresponding feedstock, which enables better inter-particle bonding resulting in more robust green parts.

### 3.7 Porosity of printed parts

Figure 12a1, b1, and c1 is the SEM micrograph of the transverse polished sections of the printed parts which were sintered in pure argon. The corresponding porosity mappings are represented by Fig. 12a2, b2, and c2. The SEM micrographs and the porosity mapping of the parts sintered in a mixture of 95% N<sub>2</sub> and 5% H<sub>2</sub> are represented in Fig. 13a1, b1, and c1 and a2, b2, and c2, respectively. Visual inspection indicated that the thermal cycle which was conducted solely with argon provided good particle sintering compared to Fig. 13a1, b1, and c1, which were sintered in a mixture of 95% N<sub>2</sub> and 5% H<sub>2</sub> and displayed inconsistent sintering and particle pull out. Porosity mapping with ImageJ quantitatively confirmed our observations, where the densification factor was above 90% when the sintering process was conducted in only argon gas for all the samples. The use of MMW PVA as a binder lead to the highest densification factor of 94.66%, which was better than the HMW and LMW binders. No literature was found which could correlate part porosity with the choice of binder. Figure 4 suggested that the burnout of the MMW PVA was more sensitive to the change in temperature and the burnout was gradual compared to the LMW and MMW PVA, leading to reduced porosity.

**Fig. 12** SEM micrograph and porosity map of parts sintered in argon environment using different modified feedstock: **a1, a2** Inconel 718 + LMW; [ $\rho_f$  = 90.23%]; **b1, b2** Inconel 718 + MMW; [ $\rho_f$  = 94.66%]; **c1, c2** Inconel 718 + HMW; [ $\rho_f$  = 92.79%]



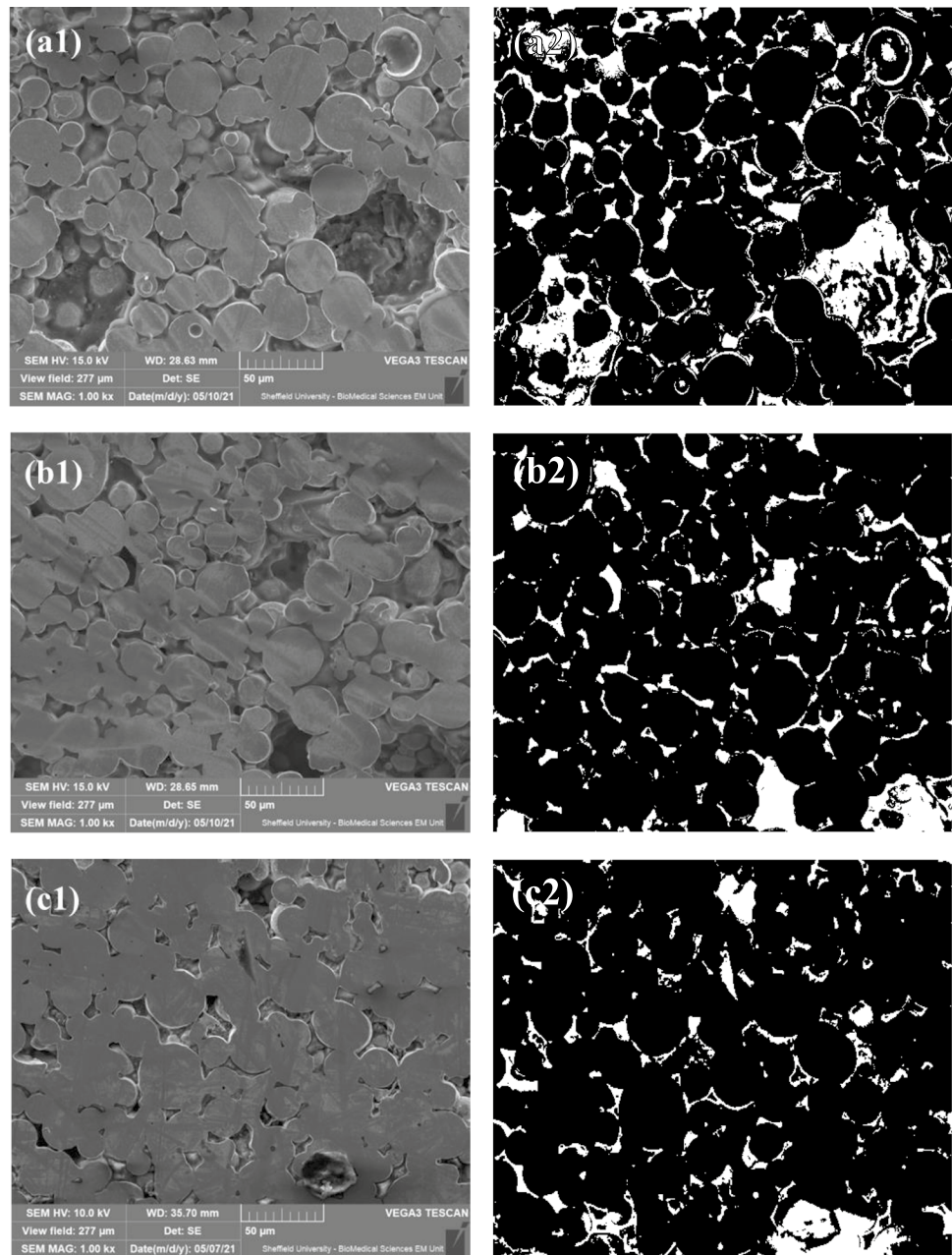
### 3.8 Mechanical properties of printed parts

Figure 14 depicts the results of the tensile testing which was performed on parts made with the three different feedstocks, namely, Inconel 718 with LMW, MMW, and HMW PVA. It was observed that parts printed with the MMW PVA had the highest ultimate tensile strength (UTS) of 246 MPa when sintered in the presence of only argon. The part using the same MMW binder but sintered in the combination of  $N_2 + H_2$  gas had a UTS of 178 MPa. The dog bones which were printed using LMW PVA as a binder underperformed with values of UTS being lower than 125 MPa for both the sintering environments. This would indicate that the

molecular weight of the PVA had a role to play in determining the tensile strength of the dog bones. The sample printed using HMW PVA and sintered solely in argon underwent a catastrophic failure and has not been presented in Fig. 14 as the failed results do not contribute to the technical discussions in any constructive manner.

The degree of influence the sintering environment has on the tensile strength of the printed parts is important as all the combinations of binders had higher values of densification factors when sintered solely in argon compared to the  $N_2 + H_2$  mix. The mixture of gases was used to discourage chromium evaporation and provide a reducing environment to neutralise the tendency for Inconel 718 to become

**Fig. 13** SEM micrograph and porosity map of parts sintered in  $N_2/H_2$  environment using different modified feedstock: **a1, a2** Inconel 718 + LMW; [ $\rho_f=82.42\%$ ]; **b1, b2** Inconel 718 + MMW; [ $\rho_f = 88.69\%$ ]; **c1, c2** Inconel 718 + HMW; [ $\rho_f =89.63\%$ ]



susceptible to oxidation above operational temperatures of 800 °C [47, 48]. It was observed that the nitrogen in the gas mixture led to nitrogen uptake by the pre-alloyed chromium to form hard and brittle  $Cr_2N$  phases, thus robbing the alloy of chromium. The presence of  $Cr_2N$  was detected by doing an X ray diffraction scan of the specimens which were sintered in the  $N_2 + H_2$  mixture. Figure 15 represents the diffraction plots of samples printed using MMW PVA in the binder and the feedstock. The specimens sintered in the  $N_2 + H_2$  mixture have  $Cr_2N$  phase detected at a  $2\theta$  value of  $63.7^\circ$ . The removal of chromium interfered with the necking ability of the particles during sintering [49] which led to incomplete sintering and poor tensile

strength. Figure 16a, b represents the SEM micrographs of the fractured surfaces of the samples sintered in  $N_2/H_2$  and only argon, respectively. The lack of necking due to nitrogen uptake can be seen in Fig. 15b. The formation of dimples, a sign of ductile fracture, is minimal with particles being pulled out from each other. Figure 16a indicated more pronounced dimpling and intra-particle fracture, which results in improved necking in between adjacent particles. There was no evidence of  $Cr_2N$  found using X ray diffraction on specimens which were sintered in the presence of argon, which resulted in proper necking action between the particles which translated in better performance during tensile testing.

**Fig. 14**  $\sigma$  vs.  $\epsilon$  curve of Inconel 718 samples printed using Inconel 718 and PVA of different molecular weights sintered in different environments

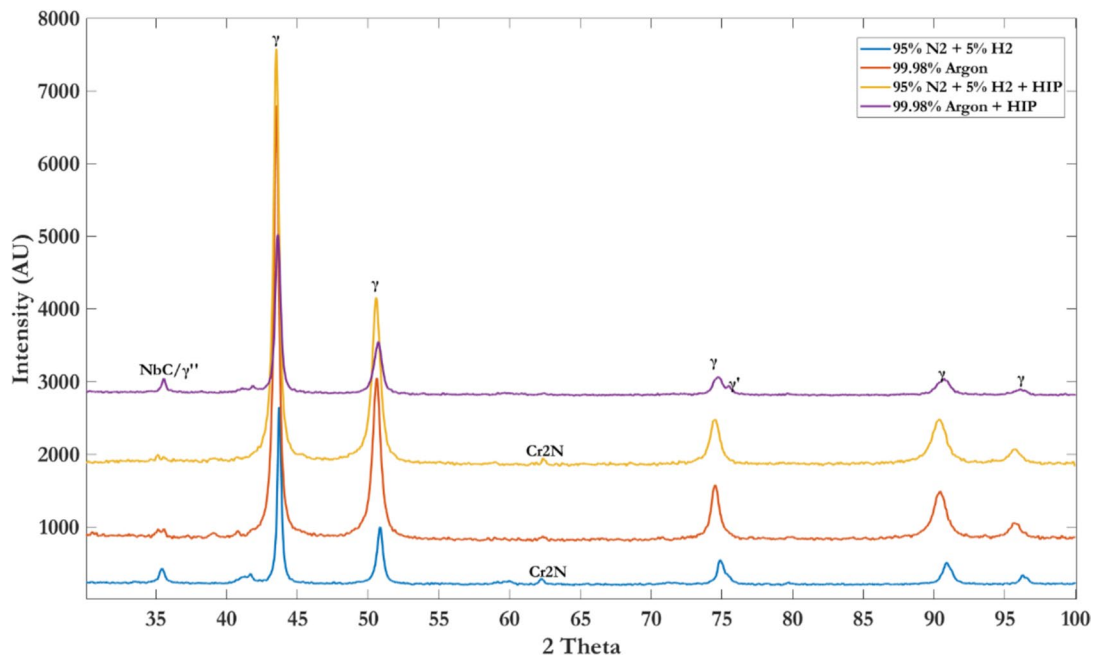
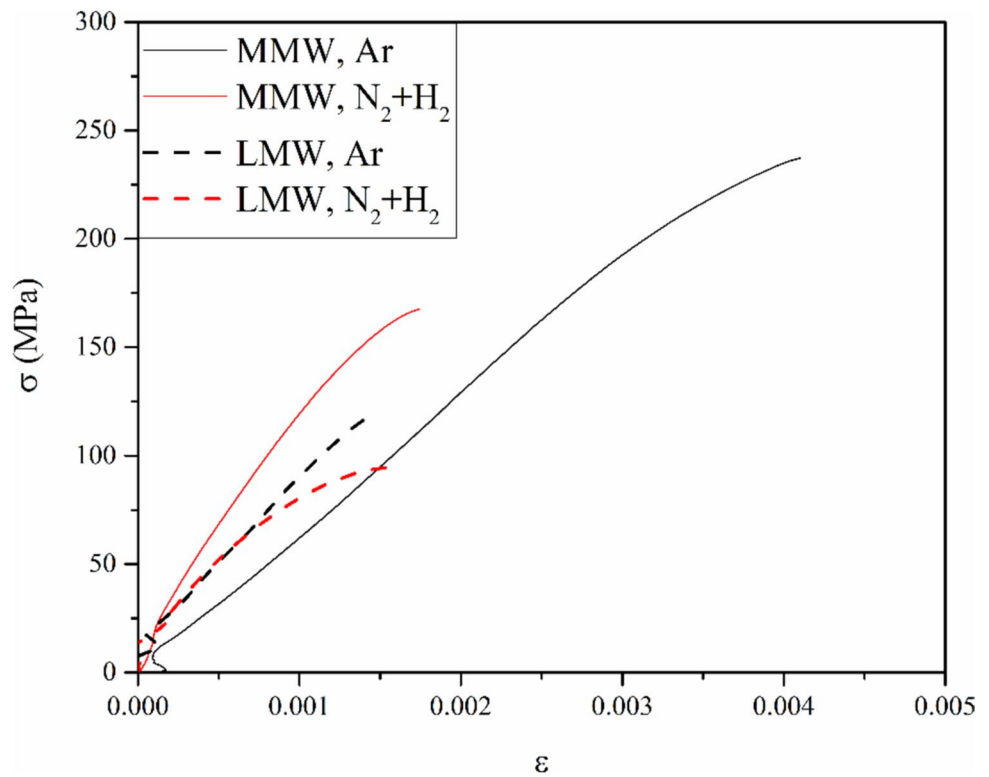


**Fig. 15** Phase analysis of samples printed with MMW PVA-based binder and feedstock with different sintering and post-processing strategies

The hardness of the sintered samples can be seen in Fig. 17. The results suggest that the samples sintered in an argon environment exhibited higher micro-hardness than their counterparts sintered in  $N_2/H_2$  gas mixture. The poor hardness was due to porosity and improper sintering seen

earlier in the samples sintered using  $N_2/H_2$ . The sample printed using the MMW PVA had the highest hardness value which was better than its HMW counterpart by a factor of 1.26.

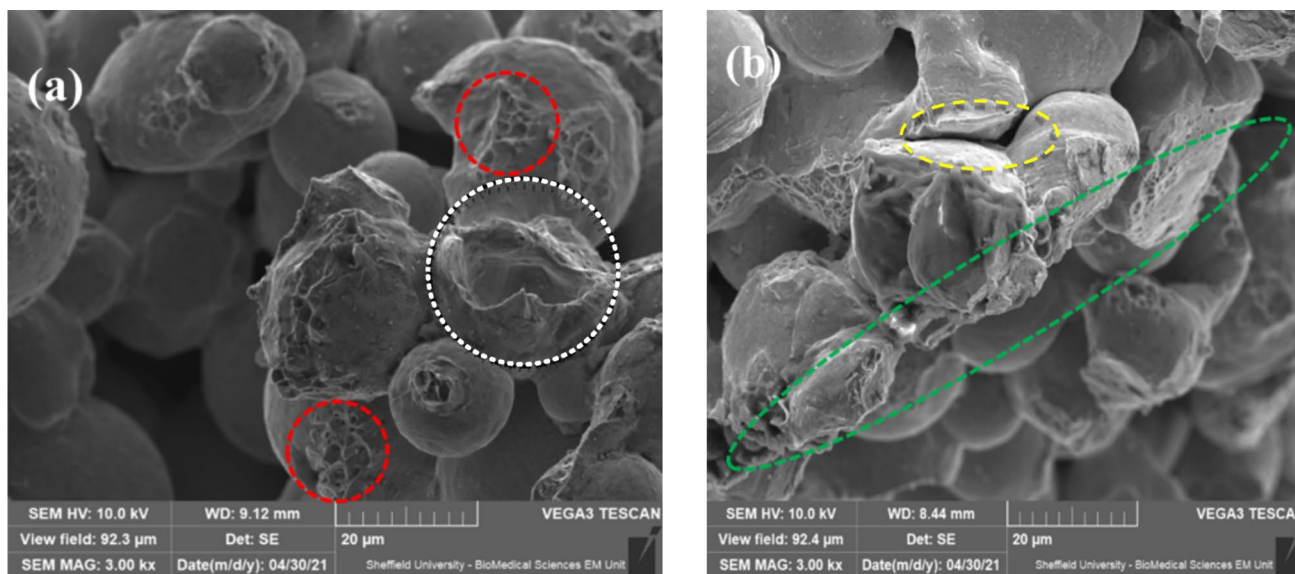


**Fig. 16** SEM of fractured surface of parts printed using Inconel 718+MMW PVA and MMW PVA binder, sintered in **a** argon and **b**  $N_2/H_2$ . The red dotted circles exhibit ‘dimpling’ which is indicative

of ductile fracture. The green dotted circles show intra-particle brittle fracture. The white dotted circles show the necking of the particle with its neighbours. The yellow dotted circle shows a lack of necking

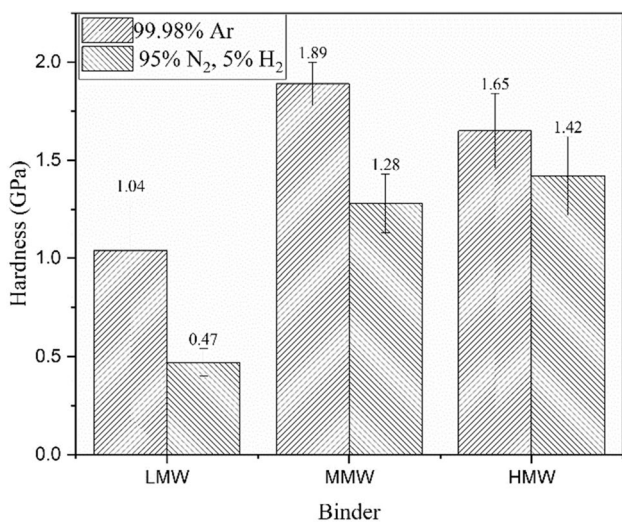


**Fig. 17** Hardness of Inconel 718 samples sintered in different environments

### 3.9 Effect of hot isostatic pressing

Figure 18 depicts the improvement in densification of parts printed using MMW and HMW PVA (5% by weight in the liquid binder and 5% by weight in the modified feedstock as dry binder) that underwent hot isostatic pressing (HIP) after being sintered in a pure argon environment. Figure 18a1, b1 represents the micrographs which reported contiguous surfaces in comparison to their pre-HIP micrographs as shown in Fig. 12b1, c1, which had discontinuities and porosity across

the surface. Figure 18a2, b2 reported densification factors of 98.96% and 98.65% for MMW and HMW PVA, respectively. The porosity of the samples after completion of HIP is at par with other studies involving commercial systems and binders where Inconel was processed using sintering procedures which are more complicated to carry out [15].

The mechanical properties of the printed Inconel 718 improved in terms of hardness and UTS as seen in Figs. 19 and 20, respectively. The samples printed using MMW binder showed an increase in hardness by 42%. The tensile samples sintered solely in argon underwent HIP and reported higher UTS than their non-HIP counterparts, which can be attributed to the improved densification which occurred in the tensile specimens’ post HIP. The MMW sample had a UTS of 1010 MPa which is like commercially available Inconel 718 which are used for load bearing applications. However, the ductile nature of the MMW sample seems to have reduced as compared to Fig. 14 as the characteristic slope which is suggestive of plastic deformation is missing.

## 4 Global synthesis of results and discussions

The characterisation of different aspects of the modified feedstock and the liquid binder was done to achieve successful jetting of a liquid binder through a piezoelectric printhead and subsequent processing of a modified feedstock which was composed of Inconel 718 powder and dry granular PVA. The initial interaction between the liquid and dry, granular PVA at room temperature was calculated to be negligible.

**Fig. 18** SEM micrograph and porosity map of parts sintered in argon environment using different modified feedstock: **a1, a2** Inconel 718 + MMW; [ $\rho_f=98.96\%$ ]; **b1, b2** Inconel 718 + MMW; [ $\rho_f = 98.65\%$ ]

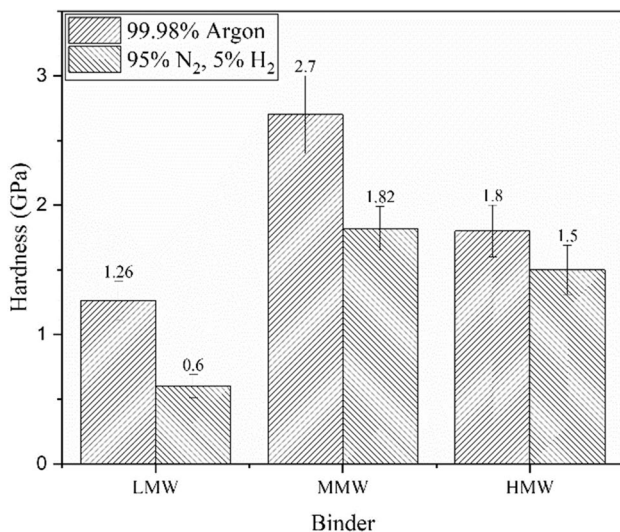
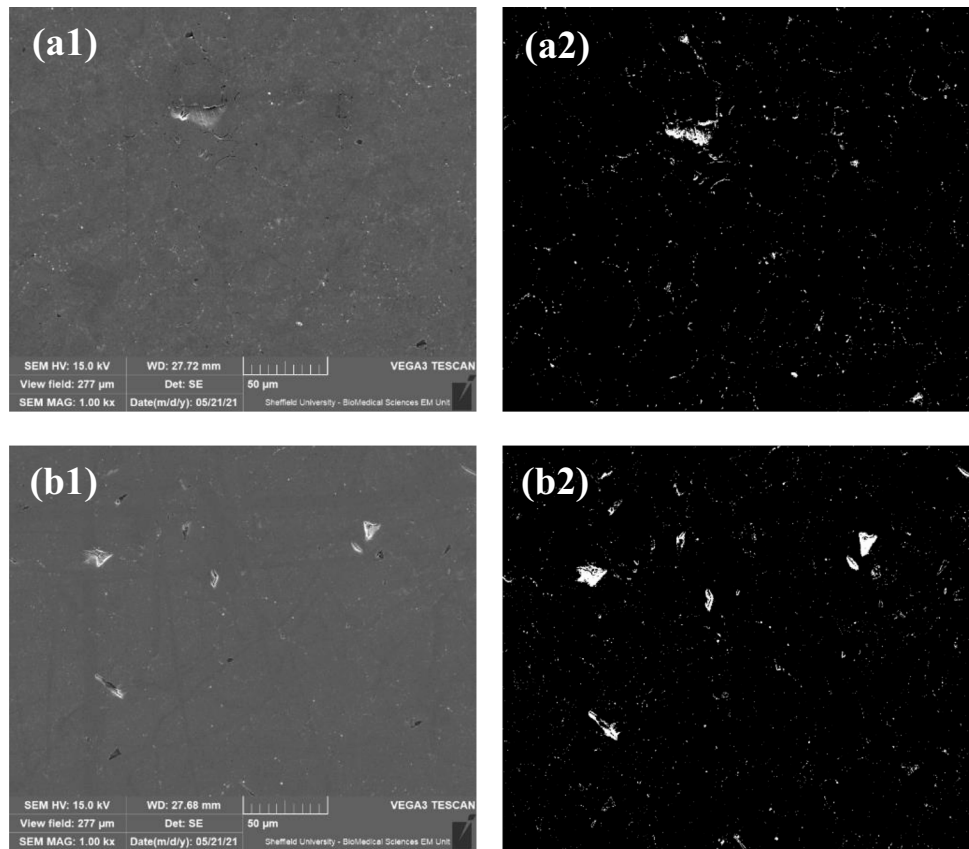


**Fig. 19** Hardness of samples sintered in different environments which underwent HIP

However, the elevated temperature during the curing stage would increase the interaction and, subsequently, the green strength of the specimens post the 12-h curing process. The role of molecular weight of the PVA on their suitability as both a dry and liquid binder was explored, and three grades of PVA—10,000 g/mol, 26,000 g/mol, and 84,000 g/mol—were

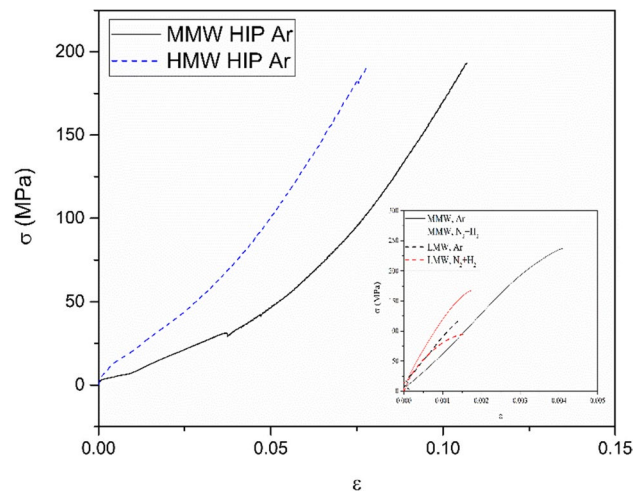


**Fig. 20**  $\sigma$  vs.  $\epsilon$  curve of Inconel 718 samples sintered in 99.98% argon which underwent HIP. Inset: Fig. 14 for purposes of comparison

taken. PVA samples having higher molecular weight were not considered considering the increased resistance to dissolution in aqueous medium when the molecular weight of PVA is between 100,000 and 150,000 g/mol [50, 51], even using water at elevated temperatures. Sessile drop testing indicated that the 5% by weight of MMW PVA had the lowest contact

angle, indicating the most conducive interaction between metal powder and liquid binder. This fact was backed up the independent results obtained after rheological evaluation of the modified feedstock and the liquid binders. The VFR rheological tests showed that the combination of dry, granular MMW PVA with Inconel 718 metal powder had the best permeability whereas the MMW based liquid binder had the best linear stability in terms of surface tension with increasing temperature. The effect of sintering environment on specimen porosity and mechanical strength was investigated. The superior interaction between the metal powder particle and MMW binder led to high densification factors when sintered in an 99.98% argon environment, but this was offset when sintered in a combination of 95% N<sub>2</sub> and 5% H<sub>2</sub> due to the formation of Cr<sub>2</sub>N which interfered with the necking process during sintering, which was visually confirmed by SEM micrography. The lack of necking and low densification in specimens sintered in (95% N<sub>2</sub> + 5% H<sub>2</sub>) environment directly contributed to poor, abrupt tensile testing and comparatively low values of UTS. The specimens which were sintered in 99.98% argon environment had lower UTS values than their formed counterparts, which quickly improved once the specimens were HIPed.

## 5 Conclusions

1. The addition of PVA increases the permeability of the resulting feedstock which would encourage better spreading of the powder. It was observed that the modified feedstocks containing 5% by weight MMW and HMW PVA had pressure drops of 5.50 mbar and 4.92 mbar, respectively, at an applied kinematic normal stress of 7.50 kPa. Pure Inconel 718 powder reported a comparatively low value of 4.37 mbar at the same kinematic normal stress of 7.50 kPa.
2. Contact angle measurements in between the liquid binders of PVA and a powder bed of virgin Inconel 718 powder revealed that the liquid binder composed of with 5% by weight MMW PVA had the lowest contact angle of 26.6° which outperformed the commercial binder's 42.4°. This was attributed to the optimal chain length of the polymer which encouraged better spreading of the binder droplet.
3. The use of MMW PVA in the feedstock in the form of granules and in the form of liquid binder also gave the

highest flexural strength of 140 N for a deflection of 0.4 mm (220 kPa), marginally outperforming its HMW counterpart which could withstand a load of 107 N for the same deflection (168.50 kPa).

4. Pure (99.98% by volume) argon gas was found to be the better sintering environment than a combination of N<sub>2</sub> (95% by volume) + H<sub>2</sub> (5% by volume) in terms of densification irrespective of the molecular weight of the PVA used in the liquid binder and modified feedstock. The densification factor,  $\rho_f$  of samples printed using MMW PVA in argon and (N<sub>2</sub> + H<sub>2</sub>) sintering environment were calculated to be 94.66% and 88.69%, respectively. The inferior performance of the combination (N<sub>2</sub> + H<sub>2</sub>) sintering environment was attributed to the uptake of N<sub>2</sub> by the Cr present in Inconel 718 which hindered inter-particle necking which occurs during the sintering process.
5. HIP of sintered samples leads to an increase in hardness and UTS. This improvement is the most marked in samples sintered solely in argon and furthermore, printed using MMW binder. The MMW sample provided a UTS of 1010 MPa which is comparable to commercially available Inconel 718.

**Acknowledgements** The authors would like to thank the EPSRC Future Manufacturing Hub in Manufacture using Advanced Powder Processes (MAPP) (EP/ P006566/1) for their support during this investigation. The authors acknowledge the help extended by Professor Ian M. Reaney in allowing them to use his sintering facility.

**Author contribution** Conceptualisation: S. Paul; data curation: S. Paul; formal analysis: S. Paul; funding acquisition: K. Mumtaz; investigation: S. Paul; methodology: S. Paul; project administration: S. Paul; supervision: K. Mumtaz and P. J. Smith; visualisation: S. Paul; drafting (original): S. Paul; and drafting (review and editing): K. Mumtaz and P. J. Smith.

**Data availability** The data that supports the findings of this study are available from S. Paul, upon reasonable request.

## Declarations

**Competing interests** The authors declare no competing interests.

**Appendix. Effect of Flory-Huggins equation on the contact angle of binder on modified feedstock** For lower molecular weight PVA:

$$n_1 = 9.99 \times 10^{-12} \text{ mol}; \phi_1 = 0.042$$

$$n_2 = 1.06 \times 10^{-8} \text{ mol}; \phi_2 = 0.958$$

Substituting the values in the Flory–Huggins equation

$$\begin{aligned} \Delta G_m^{\text{lower}} &= RT [n_1 \ln \phi_1 + n_2 \ln \phi_2 + n_1 \phi_2 \chi_{12}] \\ \Rightarrow \Delta G_m^{\text{lower}} &= 8.314 \times 303 \times [(9.99 \times 10^{-12}) \times \ln(0.042) + (1.06 \times 10^{-8}) \times \ln(0.958) + (9.99 \times 10^{-12} \times 0.958 \times 0.32)] \\ &\Rightarrow \Delta G_m^{\text{lower}} = (-0.07 \mu\text{J}) \end{aligned}$$

Similarly, for medium and higher molecular weight samples of PVA:

$$\Delta G_m^{medium} = (-0.003 \mu J)$$

$$\Delta G_m^{high} = (-0.001 \mu J)$$

**Open Access** This article is licensed under a Creative Commons Attribution 4.0 International License, which permits use, sharing, adaptation, distribution and reproduction in any medium or format, as long as you give appropriate credit to the original author(s) and the source, provide a link to the Creative Commons licence, and indicate if changes were made. The images or other third party material in this article are included in the article's Creative Commons licence, unless indicated otherwise in a credit line to the material. If material is not included in the article's Creative Commons licence and your intended use is not permitted by statutory regulation or exceeds the permitted use, you will need to obtain permission directly from the copyright holder. To view a copy of this licence, visit <http://creativecommons.org/licenses/by/4.0/>.

## References

- Sachs E, Cima M, Cornie J, Brancazio D, Bredt J, Curodeau A, Fan T, Khanuja S, Lauder A, Lee J, Michaels S (1993) Three-dimensional printing: the physics and implications of additive manufacturing. *CIRP Ann* 42(1):257–260. [https://doi.org/10.1016/S0007-8506\(07\)62438-X](https://doi.org/10.1016/S0007-8506(07)62438-X)
- Klahn C, Leutenecker B, Meboldt M (2015) Design strategies for the process of additive manufacturing. *Procedia CIRP* 36:230–235. <https://doi.org/10.1016/j.procir.2015.01.082>
- Mellor S, Hao L, Zhang D (2014) Additive manufacturing: a framework for implementation. *Int J of Prod Econ* 149:194–201. <https://doi.org/10.1016/j.jipe.2013.07.008>
- Ford S, Despeisse M (2016) Additive manufacturing and sustainability: an exploratory study of the advantages and challenges. *J Clean Prod* 137:1573–87. <https://doi.org/10.1016/j.jclepro.2016.04.150>
- Rombouts M, Kruth JP, Froyen L, Mercelis P (2006) Fundamentals of selective laser melting of alloyed steel powders. *CIRP Ann* 55(1):187–192. [https://doi.org/10.1016/S0007-8506\(07\)60395-3](https://doi.org/10.1016/S0007-8506(07)60395-3)
- Ali H, Ma L, Ghadbeigi H, Mumtaz K (2017) In-situ residual stress reduction, martensitic decomposition and mechanical properties enhancement through high temperature powder bed pre-heating of Selective Laser Melted Ti6Al4V. *Mater Sci Eng A* 695:211–220. <https://doi.org/10.1016/j.msea.2017.04.033>
- Li C, Liu ZY, Fang XY, Guo YB (2018) Residual stress in metal additive manufacturing. *Procedia CIRP* 71:348–353. <https://doi.org/10.1016/j.procir.2018.05.039>
- Vandenbroucke B, Kruth JP (2007) Selective laser melting of biocompatible metals for rapid manufacturing of medical parts. *Rapid Prototyp J* 13(4):196–203. <https://doi.org/10.1108/13552540710776142>
- Cooper K, Steele P, Cheng B, Chou K (2017) Contact-free support structures for part overhangs in powder-bed metal additive manufacturing. *Inventions* 3(1):2. <https://doi.org/10.3390/inventions3010002>
- Vaezi M, Chianrabutra S, Mellor B, Yang S (2013) Multiple material additive manufacturing—Part I: a review: this review paper covers a decade of research on multiple material additive manufacturing technologies which can produce complex geometry parts with different materials. *Virtual Phys Prototyp* 8(1):19–50. <https://doi.org/10.1080/17452759.2013.778175>
- Raza T, Andersson J, Svensson LE (2018) Microstructure of selective laser melted alloy 718 in as manufactured and post heat treated condition. *Procedia Manuf* 25:450–458. <https://doi.org/10.1016/j.promfg.2018.06.100>
- Murr LE, Gaytan SM, Ramirez DA, Martinez E, Hernandez J, Amato KN, Wicker RB (2012) Metal fabrication by additive manufacturing using laser and electron beam melting technologies. *J Mater Sci Technol* 28(1):1–14. [https://doi.org/10.1016/S1005-0302\(12\)60016-4](https://doi.org/10.1016/S1005-0302(12)60016-4)
- Zhang Y, Li Z, Nie P, Wu Y (2013) Effect of heat treatment on niobium segregation of laser-cladded IN718 alloy coating. *Metall Mater Trans A* 44:708–716. <https://doi.org/10.1007/s11661-012-1459-z>
- Popovich VA, Borisov EV, Popovich AA, Sufiarov VS, Masaylo DV, Alzina L (2017) Functionally graded Inconel 718 processed by additive manufacturing: crystallographic texture, anisotropy of microstructure and mechanical properties. *Mater Des* 114:441–449. <https://doi.org/10.1016/j.matdes.2016.10.075>
- Nandwana P, Elliott AM, Siddel D, Merriman A, Peter WH, Babu SS (2017) Powder bed binder jet 3D printing of Inconel 718: densification, microstructural evolution and challenges. *Curr Opin Solid State Mater Sci* 21(4):207–218. <https://doi.org/10.1016/j.cossms.2016.12.002>
- Utela B, Storti D, Anderson R, Ganter M (2008) A review of process development steps for new material systems in three-dimensional printing (3DP). *J Manuf Process* 10(2):96–104. <https://doi.org/10.1016/j.jmapro.2009.03.002>
- Snelling D, Williams C, Druschitz A (2014) A comparison of binder burnout and mechanical characteristics of printed and chemically bonded sand molds. In SFF Symposium, Austin. <https://doi.org/10.26153/tsw/15677>
- Hallensleben ML (2000) Polyvinyl compounds, others. *Ullmann's Encyclopedia of Industrial Chemistry*. [https://doi.org/10.1002/14356007.a21\\_743](https://doi.org/10.1002/14356007.a21_743)
- Polyvinyl chloride Safety Data Sheet No. 41243 (2008) Alfa Aesar. <https://www.alfa.com/en/msds/?language=EN&subformat=CLP1&sku=41243>. Accessed 04 December 2023
- Furan Safety Data Sheet No. A13102 (2008) Alfa Aesar. <https://www.alfa.com/en/msds/?language=EN&subformat=CLP1&sku=A13102>. Accessed 04 December 2023
- Miyajima H, Yang L (2016) Equilibrium saturation in binder jetting additive manufacturing processes: theoretical model vs experimental observations. In SFF Symposium, Austin
- Friedlander HN, Harris HE, Pritchard JG (1966) Structure–property relationships of poly (vinyl alcohol). I. Influence of polymerization solvents and temperature on the structure and properties of poly (vinyl alcohol) derived from poly (vinyl acetate). *J Polym Sci Part A-1: Polymer Chemistry* 4(3):649–664. <https://doi.org/10.1002/pol.1966.150040319>
- Kunchala P, Kappagantula K (2018) 3D printing high density ceramics using binder jetting with nanoparticle densifiers. *Mater Des* 155:443–450
- Cai J, Zhang B, Qu X (2023) Microstructure evolution and mechanical behavior of SS316L alloy fabricated by a non-toxic and low residue binder jetting process. *Appl Surf Sci* 616:156589
- ASTM standard D7981–20 (2020) ‘Standard practice for compaction of prismatic asphalt specimens by means of the shear box compactor’, ASTM International, West Conshohocken, PA, 2020
- Søgaard SV, Allesø M, Garnæs J, Baldursdóttir S, Rantanen J (2012) Development of a reproducible powder characterization method using a powder rheometer. *Annu Trans Nord Rheol Soc* 20:239–245
- ASTM standard D7334–08 (2022) ‘Standard practice for surface wettability of coatings, substrates and pigments by advancing contact angle measurement’, ASTM International, West Conshohocken, PA, 2022

28. Alghunaim A, Kirdponpattara S, Newby BMZ (2016) Techniques for determining contact angle and wettability of powders. *Powder Technol* 287:201–215
29. Zavala-Arredondo M, Groom KM, Mumtaz K (2018) Diode area melting single-layer parametric analysis of 316L stainless steel powder. *Int J Adv Manuf Technol* 94:2563–2576. <https://doi.org/10.1007/s00170-017-1040-4>
30. Valencia JJ, Spirko J, Schmees R (1997) Sintering effect on the microstructure and mechanical properties of alloy 718 processed by powder injection molding. In: E.A. Loria (Ed.) *Superalloys and various derivatives*. TMS 625:706–718
31. ASTM standard D7981–20E1131–20 (2020) ‘Standard test method for compositional analysis by thermogravimetry, ASTM International, West Conshohocken, PA, 2020
32. Lores A, Azurmendi N, Agote I, Zuza E (2019) A review on recent developments in binder jetting metal additive manufacturing: materials and process characteristics. *Powder Metall* 62(5):267–296. <https://doi.org/10.1080/00325899.2019.1669299>
33. Clayton J, Millington-Smith D, Armstrong B (2015) The application of powder rheology in additive manufacturing. *J Manuf* 67(3):544–548. <https://doi.org/10.1007/s11837-015-1293-z>
34. Lefebvre LP, Whiting J, Nijikovsky B, Brika SE, Fayazfar H, Lyckfeldt O (2020) Assessing the robustness of powder rheology and permeability measurements. *Addit Manuf* 35:101203. <https://doi.org/10.1016/j.addma.2020.101203>
35. Mohsen-Nia M, Modarress H (2006) Viscometric study of aqueous poly (vinyl alcohol) (PVA) solutions as a binder in adhesive formulations. *J Adhes Sci Technol* 20(12):1273–1280. <https://doi.org/10.1163/156856106778456636>
36. Derby B (2010) Inkjet printing of functional and structural materials: fluid property requirements, feature stability, and resolution. *Annu Rev Mater Res* 40:395–414. <https://doi.org/10.1146/annurev-matsci-070909-104502>
37. Tekin E, Smith PJ, Schubert US (2008) Inkjet printing as a deposition and patterning tool for polymers and inorganic particles. *Soft Matter* 4(4):703–713. <https://doi.org/10.1039/B711984D>
38. Vadillo DC, Tuladhar TR, Mulji AC, Mackley MR (2010) The rheological characterization of linear viscoelasticity for ink jet fluids using piezo axial vibrator and torsion resonator rheometers. *J Rheol* 54(4):781–795. <https://doi.org/10.1122/1.3439696>
39. Stevens E, Schloder S, Bono E, Schmidt D, Chmielusz M (2018) Density variation in binder jetting 3D-printed and sintered Ti-6Al-4V. *Addit Manuf* 22:746–752. <https://doi.org/10.1016/j.addma.2018.06.017>
40. Miyanaji H, Zhang S, Yang L (2018) A new physics-based model for equilibrium saturation determination in binder jetting additive manufacturing process. *Int J Mach Tools Manuf* 124:1–11. <https://doi.org/10.1016/j.ijmactools.2017.09.001>
41. Sengwa RJ, Kaur K (2000) Dielectric dispersion studies of poly (vinyl alcohol) in aqueous solutions. *Polym Int* 49(11):1314–1320. [https://doi.org/10.1002/1097-0126\(200011\)49:11%3c3C1314::AID-PI479%3e3E3.0.CO;2-8](https://doi.org/10.1002/1097-0126(200011)49:11%3c3C1314::AID-PI479%3e3E3.0.CO;2-8)
42. Kozlov M, McCarthy TJ (2004) Adsorption of poly (vinyl alcohol) from water to a hydrophobic surface: effects of molecular weight, degree of hydrolysis, salt, and temperature. *Langmuir* 20(21):9170–9176. <https://doi.org/10.1021/la0492299>
43. Flory PJ (1942) Thermodynamics of high polymer solutions. *J Chem Phys* 10(1):51–61. <https://doi.org/10.1063/1.1723621>
44. Huggins ML (1942) Some properties of solutions of long-chain compounds. *J Phys Chem* 46(1):151–158. <https://doi.org/10.1021/j150415a018>
45. Miyanaji H, Orth M, Akbar JM, Yang L (2018) Process development for green part printing using binder jetting additive manufacturing. *Front Mech Eng* 13:504–512. <https://doi.org/10.1007/s11465-018-0508-8>
46. Zhou Z, Lennon A, Buchanan F, McCarthy HO, Dunne N (2020) Binder jetting additive manufacturing of hydroxyapatite powders: effects of adhesives on geometrical accuracy and green compressive strength. *Addit Manuf* 36:101645. <https://doi.org/10.1016/j.addma.2020.101645>
47. Jones WR (1997) Partial pressure vacuum processing-part I. *Ind Heat-Pittsburgh Troy* 64:119–121
48. Jones WR (1997) Partial pressure vacuum processing-part II. *Ind Heating-Pittsburgh Troy* 64:122–126
49. Saha D (2001) De-lubrication during sintering of P/M compacts: operative mechanism and process control strategy (Report No. 01-2) [Masters Dissertation, Worcester Polytechnic Institute]. Digital WPI
50. Limpan N, Prodpran T, Benjakul S, Prasarnpran S (2012) Influences of degree of hydrolysis and molecular weight of poly (vinyl alcohol) (PVA) on properties of fish myofibrillar protein/PVA blend films. *Food Hydrocolloids* 29(1):226–233. <https://doi.org/10.1016/j.foodhyd.2012.03.007>
51. Stevens MP (1999) *Polymer chemistry: an introduction*, 3rd edn. Oxford University Press. [https://pearl-hifi.com/06\\_Lit\\_Archive/14\\_Books\\_Tech\\_Papers/03\\_Polymer\\_Science/03\\_Polymer\\_Chemistry\\_An\\_Introduction\\_3rd\\_Edin.pdf](https://pearl-hifi.com/06_Lit_Archive/14_Books_Tech_Papers/03_Polymer_Science/03_Polymer_Chemistry_An_Introduction_3rd_Edin.pdf)

**Publisher's Note** Springer Nature remains neutral with regard to jurisdictional claims in published maps and institutional affiliations.